

## Halloysite nanoparticles of detritus from mangrove-estuarine ecosystem: Potential as antibacterial agents and wound healing activity

Munmun Mallik Ghosh<sup>1</sup>, Swarnali Das<sup>2</sup>, Santi M. Mandal<sup>3</sup>, Susanta K. Chakraborty<sup>1</sup>

<sup>1</sup>Department of Zoology, Vidyasagar University, Midnapore 721102, West Midnapore, India

<sup>2</sup>Department of Metallurgical & Materials Engineering, IIT Kharagpur, Kharagpur, West Bengal, India

<sup>3</sup>Central Research Facility, Indian Institute of Technology Kharagpur, Kharagpur 721302, West Bengal, India

(Received: June 2019      Revised: August 2019      Accepted: September 2019)

Corresponding author: **Santi M. Mandal**. Email: munmun1008@gmail.com

### ABSTRACT

**Introduction and Aim:** Halloysite nanoparticles are emerging in drug delivery in recent years because of their high level of biocompatibility. Chronic nonhealing wounds pose a substantial economic burden on health care systems. The chronic and complicated nature of nonhealing wounds has led to the development of several nanotechnology-based therapies. The present study aims at finding a suitable biomedical application of the unique shaped halloysites obtained from the detritus of the estuarine mangrove ecosystem.

**Materials and Methods:** Halloysite nanoparticles are purified after collecting from the intertidal soils of mangrove-estuarine ecosystem in eastern India and characterized following standard methods using a transmission electron microscope, X-Ray Diffraction technique and Fourier Transform Infrared Spectroscopy. After that boric acid was conjugated to halloysite because they significantly get loaded into the halloysite nanoparticle and these newly formed biochemical entities have been observed to increase the antibacterial activity as revealed by scanning electron microscopic studies.

**Results:** Transmission electron microscopy and X-ray diffraction studies have revealed that the detritus from the estuarine mangrove ecosystem contains halloysite nanoparticles. The nanoparticles are rod-shaped and amorphous. Fourier Transform Infrared Spectroscopy has also shown that the particles are halloysite, mainly composed of both minerogenic (aluminum silicates) as well as organic (humic substances containing phenolic OH) substances. This halloysite conjugated boric acid is a fast healer of the burn-induced wound in male Swiss albino mice. Results derived from the release kinetics have highlighted the removal of boric acid totally from the conjugate halloysite within 5 minutes in the presence of 0.5% H<sub>2</sub>O<sub>2</sub>.

**Conclusion:** Thus, this natural biocompatible halloysite particle, chemically identical to kaolinite structure characterized in having free hydroxyl groups, finds a wide range of nanotechnology-based applications, especially for capturing drug and sustained release in biomedical applications.

**Key words:** Nanoparticles; halloysites; mangrove-estuarine ecosystem; detritus; biomedical applications.

### INTRODUCTION

Natural soil textural components, especially clay, play a vital role in human health (1), including warfare (2, 3). Clay nanoparticles find wide application as safe and natural drug delivery agents (4, 5). There have been several reports describing the wound healing properties of natural and synthetic clay minerals (6-8). They act as antibacterial agents, drug delivery vehicles, and thereby contribute as wound healing agents. Despite these studies and the clinical evidence suggesting that clay minerals promote healing in individuals, the mechanism by which the clay minerals exhibit such properties mostly remains unknown.

Halloysite is a naturally occurring member of the kaolin family of aluminosilicate clays. Halloysite can occur in several structures but predominantly exists as

a tubular structure, which is believed to be formed by hydrothermal alteration, or surface weathering of other aluminosilicate minerals (9). The chemical formula of halloysite and kaolinite is similar, Al<sub>2</sub>Si<sub>2</sub>O<sub>5</sub>(OH)<sub>4</sub>.nH<sub>2</sub>O, but structurally halloysite differs by possessing a hollow tubular structure (halloysite nanotube) (9, 10), the luminal diameter of which is 10 to 15 nm with an outside diameter ranging from 50 to 70 nm and a length between 500 and 2000 nm (11). The halloysite wall is composed of 10–15 bilayers of aluminum and silicon oxide. A difference in chemical composition at both the inner and outer surface gives it a net negative charge at the pH ranging from 2 to 10. The vast surface area of this nanotube (around 57 m<sup>2</sup>/g), along with luminal porosity, indicates its significant potential for binding and releasing of

biologically functional molecules such as drugs, proteins, DNA, growth factors, etc.

Halloysite nanotubes provide a new avenue for the preparation of nanocomposites (12). It can be mined from natural deposits in many countries such as America, Brazil, China, Japan, Turkey, Thailand, Indonesia, and New Zealand, including India (13). In chronic wound management, the topical use of antibiotics has become a central issue due to the increasing incidences of drug-resistant microbes. Chronic nonhealing wounds pose a substantial economic burden on health care systems (14). In a recent study on wounds in India, we have found that the prevalence of acute and chronic wounds was 10.55 and 4.48 per 1000 of the population, respectively (15). Researchers across the globe explore several alternative therapies for wound healing. The chronic and complicated nature of nonhealing wounds has led to the development of several nanotechnology-based therapies. To find an effective, safe, and low-cost solutions to treat and manage acute and nonhealing wounds, we have undertaken the present study to assess the potential of clay-based halloysite nanoparticles on healing burn-induced wounds in mice.

## **MATERIALS AND METHODS**

### **Sample collection**

Intertidal sediment covered with surface detritus was collected from the confluence of Subarnarekha River with the Bay of Bengal, an ecotone located at the junction of Midnapore (East), West Bengal, India and at Talsari, Odisha, India.

### **Sample preparation**

The collected moist field sediment samples were dried at room temperature and stored in airtight containers. 10 grams of the dried and grained sediment sample was dissolved into 20ml methanol (100%) in a tube, vortexed for 10 minutes, and allowed to settle. The sample was then decanted very carefully into a 50 ml centrifuge tube and subsequently centrifuged at 4700 rpm for 20 minutes. The supernatant removed, the residue is left to dry, and the dried materials were collected. Dry pellets of the residues were further powdered in mortar and pestle and preserved at room temperature.

### **Characterization**

Fourier Transform Infrared (FTIR) spectra of the samples are recorded on a Thermo Nicolet NEXUS-870TM spectrophotometer using a KBr pellet. The morphology and microstructure of the samples are obtained using an FEI- TECHNAI G2 20S – TWIN analytical Transmission Electron Microscope. Powder X-Ray Diffraction (XRD) analyses were performed

using a diffractometer with Cu anode (PAN analytical X'pert PRO), running at 40 k V and 30 mA, scanning from 2 to 80° for 10 minutes. Field Emission Scanning Electron Microscope (FESEM), model- ZEISS EVO 60 (Merlin SEM) is used to study the antibacterial effect against two bacterial species, *Staphylococcus aureus*, a skin pathogen, and *Escherichia coli*, a gut microbe.

### **Antibacterial assay**

The boric acid conjugated halloysite is tested for antibacterial assay. The antibacterial activity of the halloysite nanoparticle is tested using two different bacterial strains. Bacterial cells are treated with boron conjugated halloysites, and changes observed in surface topology are recorded by SEM analysis.

### **Sample preparation for SEM**

To ninety microliters (90µl) of each bacteria culture, 10 µl of halloysite nanoparticles and 10 µl of boric acid loaded halloysite (in 1:1 ratio) were added in separate tubes and kept in room temperature for 24 hours. The samples were then run through the acetone gradient for rehydration. 10 µl of glutaraldehyde is added to the remaining pellet after vortexing for 5 minutes, and the mixture is centrifuged for 2 min at 13000 rpm. The pellet was resuspended in 40 µl of 40% acetone and, allowed to vacuum dry after being drop cast over glass coverslip before analysis.

### **Sample preparation for FTIR**

Three milligrams (mg) of dried powder was mixed in 300 mg of KBr. These were homogenized by mixing in a stainless-steel vibrating mill. The mixed samples were then poured into stainless steel cups, having a diameter of 10 mm, and the top surfaces of the powders leveled. Spectra were recorded for infrared measurement from 4000 to 500 cm<sup>-1</sup> at 1.92 cm<sup>-1</sup> interval.

### **Sample preparation for TEM**

One drop of the diluted sample in MeOH is pipetted out on a copper grid and dried. The dried samples are studied in an FEI- TECHNAI G2 20S – TWIN ANALYTICAL TEM, operated at an accelerating voltage of 200 kilovolts.

### **Sample preparation for wound healing assay**

To 300µl of water solution of each sediment sample, 100µl of boric acid of the same concentration (40mg/ml) was added and shaken well.

### **In vivo assay**

The study was performed on five male Swiss albino mice, weighing 30.0-1.0 g and one animal per cage. Cages spreaded with rice straw were kept in animal enclosure, maintaining proper conditions of

temperature (25± 2°C), humidity (55 ± 5%), and photoperiod (12 h). Throughout the experiment, the animals consumed water and food ad-libitum (30).

### Burning procedure

In the present study, the method of burning followed was similar to earlier reported methods, with little modifications (16). The mice were anesthetized by an intraperitoneal injection of ketamine HCl (35 mg/kg). The fur/hairs were shaved using sterile scissors and razors from the body parts of the animals, where burning was intended. A fire protective cloth was held tightly over the shaved region, having a window of 1 cm on the back of the anesthetized animal followed by a spreading of 0.2 ml of 95% ethanol, and then it was burned for 15 seconds. The animals were infected in the burnt area by inoculating with the bacteria, *Staphylococcus aureus*, causing external infection at the burn wound site.

### Topical treatment of burn afflicted site

Drug materials for treatment are applied after completion of the external infection. Wounds are inflicted in two mice, on either side of each mouse. In one mouse, the boric acid conjugated halloysite is applied while the other is treated with sterile PBS buffer. The dosage of the application was 20 µl administered on the right-side wound, the concentration of the drug being 40 mg/ml in water solution. All the wounds were examined regularly and photographed at 24 hours interval for further observation and recordings.

### Drug loading and release method

## RESULTS

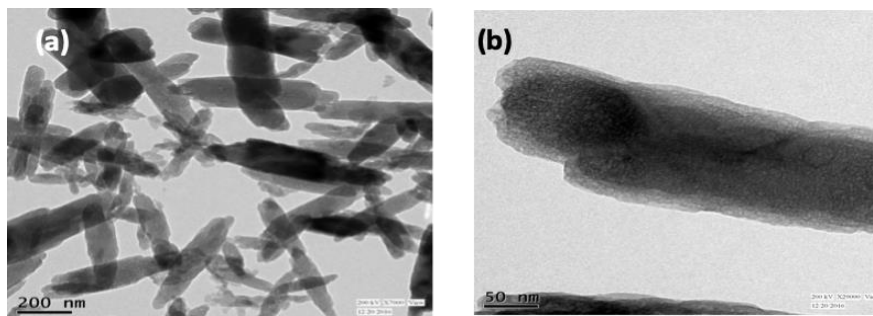


Fig.1 a) TEM images of powdered detritus sample, (b) Magnified image of the powdered sample.

### Microanalysis report

Microstructure analysis reveals that the estuarine detritus constitutes of the mineral halloysite having a unique size and shape, as is evident in Fig. 1(a, b). The

Halloysite nanoparticle incorporating boron is prepared in water solution. Five-milligram of halloysite was dissolved in 1mL double distilled water and stirred. Then 20 µl Boric acid of 4 mg/ml concentration was dissolved in 80µl water. The solution was then transferred to a 2000 Da molecular weight cutoff dialysis bag and dialyzed for 14 hours to remove the impurities and free boron. The absorbance of the halloysite solution is measured at 328 nm by UV-Visible spectrophotometer. Then absorbance of different concentrations of boron loaded halloysite drug was measured. A calibration curve was constructed using different concentrations (1–100 µg/mL) of free drug in a buffer. Drug loading content (DLC) is calculated from the following equation:

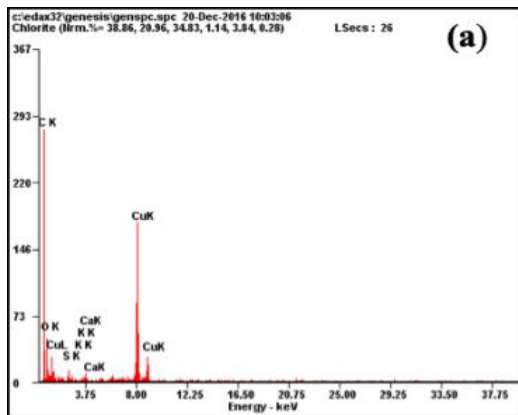
$$\text{DLC (\%)} = (\text{Wt. of loaded drug} / \text{Wt. of drug-loaded halloysite}) \times 100$$

The *in vitro* drug release profile is obtained. 30µl boron loaded halloysite was sealed in a dialysis tube (molecule cutoff 3,000) and incubated at 27 °C under stirring at a speed of 80 rpm. At regular time intervals, the 1ml of the mixture was removed and replaced by fresh PBS to maintain sink conditions. After adding H<sub>2</sub>O<sub>2</sub> in boron loaded halloysite, drug concentration in solution was calculated by measuring absorbance in UV-Visible spectrophotometer at a time interval of 0 minutes, 2 minutes, 4 minutes, 8 minutes, 12minutes, 16 minutes, 20 minutes, 24 minutes, 28 minutes and 32 minutes. Drug release was calculated by the following equation:

$$F_t = C_t / C_0$$

Where, F<sub>t</sub> is functions of drug release, C<sub>t</sub> is drug release at time t, and C<sub>0</sub> is initial drug release time.

weight and atomic percentages of the elements present in halloysite are also expressed in the microanalysis report; Fig. 2(a, b).



Element	Wt %	At %
C K	39.11	47.14
O K	55.09	49.85
Na K	02.58	01.62
Mg K	00.17	00.10
Si K	00.03	00.02
S K	02.13	00.96
K K	00.07	00.03
Ca K	00.70	00.25
Cu K	00.12	00.03

Fig. 2: Microanalysis report (a) Graph showing elements present in the sample, (b) Table showing weight and atomic percentages of those elements.

**Antibacterial assay**

The drug halloysite loaded boric acid shows the bacteriocidal effect when applied to both the bacteria, *Escherichia coli*, and *Staphylococcus aureus* while the

maximum inhibitory effect was observed in *Staphylococcus aureus* as shown in Fig. 3 (a, b) and 4 (a, b).

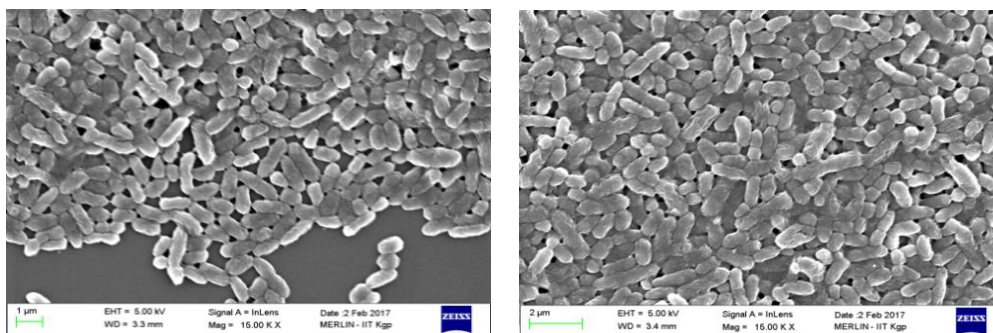


Fig. 3: (a) *E. coli* treated with sediment (b) *E. coli* treated with sediment of halloysite loaded with boric acid

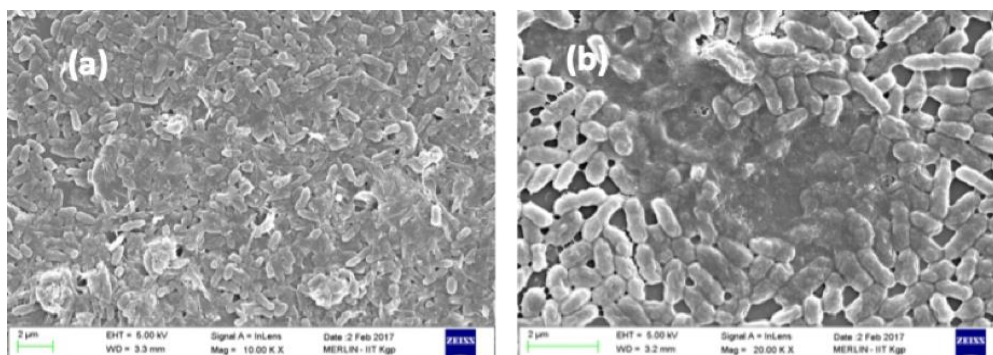


Fig. 4: (a) *Staphylococcus aureus* treated with sediment (b) *Staphylococcus aureus* treated with sediment of halloysite loaded with boric acid

**Analysis of the FTIR spectrum**

Several bands have been detected in the FTIR spectra in the range of 400 to 4000  $cm^{-1}$ . Each peak corresponds to a vibration line that, in turn, is assigned to a stretching or deformation of functional groups. The spectra of halloysite exhibited a range of 650-1350  $cm^{-1}$  which is similar to that of kaolinite (17). Bands for mineralogic and organic materials were within 900-1200  $cm^{-1}$ ; for amides and carboxyl groups

were within 1500-1800  $cm^{-1}$  and for humic compounds were within 2800-3450  $cm^{-1}$  depicting organic materials with functional groups containing various C-H components and 3700  $cm^{-1}$  is of Si-OH. The range of 1500-2000  $cm^{-1}$  was previously used to characterize humic substances and marine sediments (18). The intense bands at 1733  $cm^{-1}$  and 1638  $cm^{-1}$  (Fig. 5a) are characteristic peaks of humic acids (HA) and fulvic acids (FA), respectively. The first intense absorption band at 1733  $cm^{-1}$  is characterized as C=O stretching

vibration of carboxylic acid groups, while the chemistry of the second band is interpreted as the mixture of the stretching vibrations of C=C aromatic bonds, conjugated carbonyl groups (quinone), carboxylic salt groups and amide groups. Another crucial feature is the characteristic peak of the lignin spectrum, which can be assigned to an aromatic C=C stretching vibration in the interval of 1544–1511cm<sup>-1</sup>.

In general, silicate minerals absorb in the range of 815-1300 cm<sup>-1</sup>, mainly due to Si-O stretching. The Si-O stretching is confirmed by the presence of absorption bands at 1191 cm<sup>-1</sup>, 1104 cm<sup>-1</sup>, and 1045 cm<sup>-1</sup> as in Fig. 5a. The vibration around 1630 cm<sup>-1</sup> is common for hydrated phyllosilicates (e.g., chlorite, illite, smectite, and halloysite) corresponds to the H-O-H stretching bonds of absorbed water. Similarly, the overall positive loadings in the water absorbance-related region (2856-3716 cm<sup>-1</sup>), particularly high-intensity band at 3450 cm<sup>-1</sup> (Fig. 5a) of halloysite from our study site are related to water absorption bands. Thus, an FTIR

spectroscopy makes it possible to identify clay minerals from the selected site reliably.

### Analysis of XRD data

Figure 5b shows the XRD pattern of the synthesized halloysite nanomaterials using a Cu target (1.541838 Å). Using the software, X-pert high score, we have identified the presence of hydrated halloysite crystal structure in conjunction with some other additional phases, such as SiO<sub>2</sub>, Na<sub>2</sub>SO<sub>4</sub>, K<sub>2</sub>Ca<sub>2</sub>(SO<sub>4</sub>)<sub>3</sub>, Na<sub>1.3</sub>K<sub>0.7</sub>Si<sub>2</sub>O<sub>5</sub>, Na<sub>2</sub>S<sub>2</sub>O<sub>3</sub>. The peaks of halloysite-10 Å phase at 19.89°, 35.02°, 40.4°, and 54.93° correspond to (020), (200), (203), (044) plane, respectively. The crystallographic d spacing from these planes is 0.44, 0.25, 0.18, and 0.16 nm, respectively. The crystallite size is calculated from Debye-Scherrer equation ( $\tau = 0.89 \lambda / \beta \cos \theta$ ) where  $\lambda$ ,  $\beta$ ,  $\theta$  are the wavelength of X-ray, line broadening at half the maximum intensity (FWHM) and Bragg angle respectively. The typical value of halloysite crystallite size is found ~ 25.2 nm using 2 $\theta$  ~35° peak Bragg angle and Gaussian fitting as is evident from Fig. 5c.

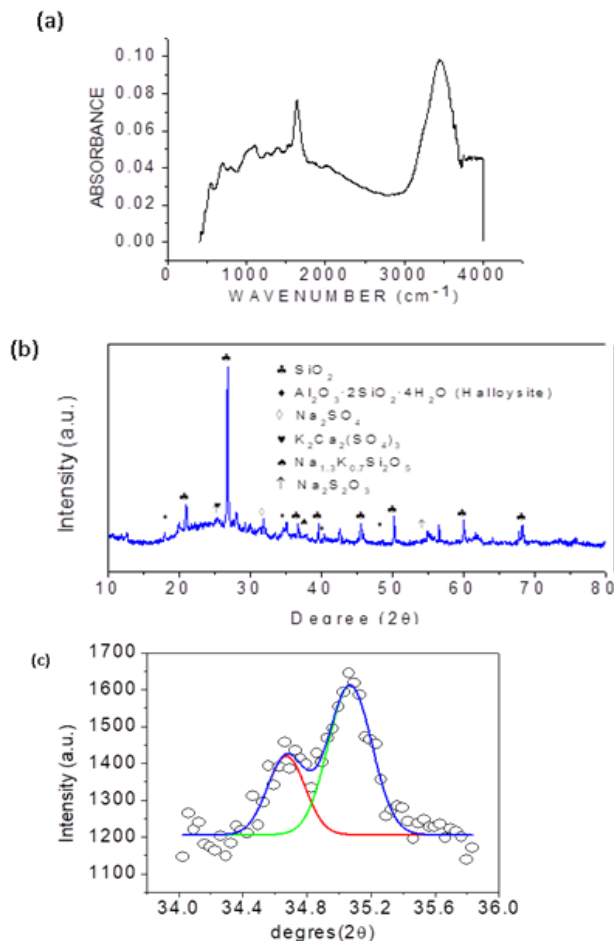
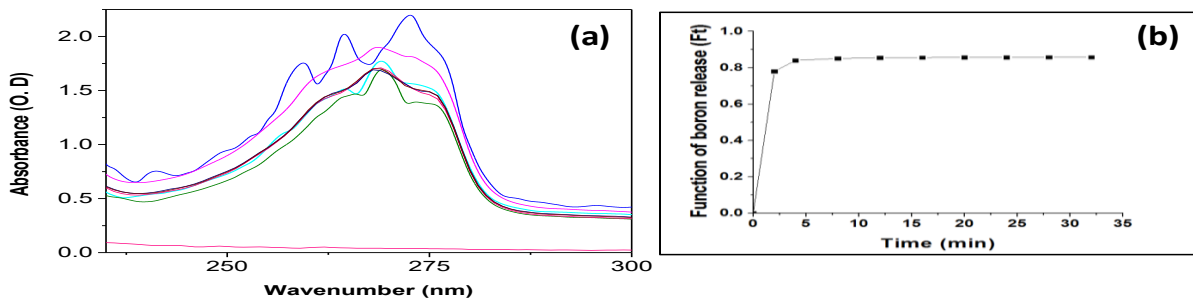


Fig. 5: (a) FTIR spectrum for sample, (b) X-Ray Diffraction pattern of powdered sample (c) The experimental (dotted) and fitted (line) for evaluating the crystallite size of halloysite crystal.

**Drug loading and release of clay conjugated boric acid**

The pure halloysite shows the absorbance spectrum of the high-intensity band at 263nm, 270nm, and 276 nm (Fig. 6a). This spectrum is due to the conformational changes in the aqueous solvent, which, have different molecular interactions within their self-aggregation structure. There is an increase in the shift of absorption peak at a lower wavelength with a higher order of self-aggregation by forming a complex with other molecules. The absorption spectrum of boron loaded halloysite conjugate shows a hypsochromic shift from

263nm,270nm, and 276 nm to 258nm, 264nm, and 272nm respectively at 5% boron loading which can be attributed for the higher-order association of boron in an aqueous solution that becomes entrapped inside the halloysite conjugate. At 10% boron loading bands obtained are 254nm, 262nm, and 269nm. With further increase in concentration (15%, 20%, 25%, and 30%), no changes in the shift are found, signifying saturation at 10% solution of boron. Boric acid is removed from the halloysite conjugate within 5 minutes in the presence of 0.5% H<sub>2</sub>O<sub>2</sub>. The release kinetics presented in Fig. 6b.



**Fig. 6:** (a) Loading of boron halloysite based drug (b) release kinetics of boron halloysite based drug

**In vivo assay**

In the animals treated with halloysite loaded boric acid, the pathogen-load for the bacteria, *Staphylococcus aureus*, progressively reduced as is shown in Fig. 7(a,

b, c). The treated animals almost healed in the 20th day following the burn, while viable bacteria were still observed in the burn wounds of the untreated animals.



**Fig. 7:** Progress of infected (*Staphylococcus aureus*) burn-wound healing (a) wound at Day 3, (b) wound at Day 10, (c) wound at Day 20

**DISCUSSION**

Recent research trends find halloysites as nano-sized drug delivery vehicles. Halloysites are natural biocompatible nanoparticles generally obtained from mineral deposits throughout the world. The source of halloysite from the detritus in the present study is unique because of the uniqueness of the estuarine mangrove ecosystem, where the decomposition of plant litters produces a vast amount of detritus through the interactions of an array of organisms (benthos, microbes, etc.,). Also, those litter contributed detritus are transported from the mangrove forest subsystem to the adjoining estuarine water flows in order to ensure maximum biological productivity of the mangrove-estuarine ecosystem (19, 20). Estuarine regions being a confluence of rivers with the sea having tidal

fluctuations-deposit sediments from the flowing water having different textural and nutrients contents (21, 22). All those deposited sediments after being mixed up with plant debris contributed to detritus display diverse molecular compositions. This deposition may be due to the erosion of many rock and mineral deposits caused by rivers while flowing through its catchment area. These rocks and minerals mix up with plant-derived detritus, which with time through several natural and ecological interaction processes, are supposed to form halloysites after being deposited in the bottom. Estuarine sediments experience a lot of biological and physicochemical interactions due to the influence of Eco dynamics. This involves the influence of interactions between different floral and faunal components, microbes, physical and chemical characteristics of air (wind flow, atmospheric density,

particulate load, rainfall, humidity, temperature etc.), soils (texture, nutrients etc.) and water (pH, temperature, nutrients, turbidity etc.) on the sediments. So finally, this may account for the development of the uniqueness of the size and shape of halloysites (not yet been reported earlier) used in the present research. The halloysite used for the present research contains both organic and inorganic fractions, as reported by earlier researchers.

Boric acid found as a constituent of many naturally occurring minerals, plants, and seawater, is often used as a broad-spectrum antiseptic (23). It is a weak tribasic Lewis acid of boron forming diols when combined with halloysites' free hydroxyl groups. The third hydroxyl group of boric acid remains free to exhibit its antibacterial properties. Poor wound healing resulting from trauma, surgery, acute illness, or chronic disease conditions affects humanity throughout history. The repair of wounds is one of the most complex biological processes that occur in our body (24). Regeneration and tissue repair processes consist of a cascade of molecular and cellular events that starts after the wounding in order to restore the damaged tissue. These cellular events lead to differentiation, proliferation of myofibroblast, and the consequent migration of fibroblasts and keratinocytes, leading to collagen synthesis and maturation, re-epithelialization, and angiogenesis (25). Failure of one or several cellular processes leads to chronic wounds. The halloysite conjugated boric acid when used as a wound-healing agent in mammalian mice model has been found to heal wounds as efficiently as other halloysite based drugs but in a more economical and effective manner.

## REFERENCES

1. Viseras, C., Aguzzi, C., Cerezo, P., Lopez-Galindo A., Uses of clay minerals in semisolid health care and therapeutic products. *Applied Clay Science*. 2007; 36(1); 37-50.
2. Josse, D., Wartelle, J., Cruz, C., Showering effectiveness for human hair decontamination of the nerve agent VX. *Chemico-Biological Interactions*. 2015; 232; 94-100.
3. Matar, H., Guerreiro, A., Piletsky, S. A., Price, S. C., Chilcott, R. P., Preliminary evaluation of military, commercial and novel skin decontamination products against a chemical warfare agent simulant (methyl salicylate). *Cutaneous and Ocular Toxicology*. 2016; 35(2); 137-144.
4. Jafarbeglou, M., Abdouss, M., Shoushtari, A. M., Clay nanocomposites as engineered drug delivery systems. *RSC Advances*. 2016; 6(55); 50002-50016.
5. Zhang, Y., Long, M., Huang, P., Yang, H., Chang, S., and Hu, Y., et al., Intercalated 2D nanoclay for emerging drug delivery in cancer therapy. *Nano Research*. 2017; 10(8); 2633-2643.
6. Gaskell, E. E., Hamilton, A. R., Antimicrobial clay-based materials for wound care. *Future Medicinal Chemistry*. 2014; 6(6); 641-655.
7. Emami-Razav, S. H., Esmaeili, N., Forouzannia, S., Amanpour, S., Rabbani, S., Alizadeh, M., et al., Effect of Bentonite on skin wound healing: Experimental study in the rat mode. *Acta Medica Iranica*. 2005; 44(4); 235-240.
8. Morrison, K. D., Misra, R., Williams, L. B. Unearthing the Antibacterial Mechanism of Medicinal Clay: A Geochemical Approach to Combating Antibiotic Resistance. *Scientific Reports*. 2016; 6; 19043.
9. Guimarães, L., Enyashin, A. N., Seifert, G., Duarte, H. A., Structural, Electronic, and Mechanical Properties of Single-Walled Halloysite Nanotube Models. *The Journal of Physical Chemistry C*. 2010; 114(26); 11358-11363.
10. Levis, S. R., Deasy, P. B., Use of coated microtubular halloysite for the sustained release of diltiazem hydrochloride and propranolol hydrochloride. *International Journal of Pharmaceutics*. 2003; 253(1); 145-157.
11. Abdullayev, E., and Lvov, Y., Halloysite Clay Nanotubes for Controlled Release of Protective Agents. *Journal of Nanoscience and Nanotechnology*. 2011; 11; 10007-10026.
12. Vinokurov, V. A., Stavitskaya, A. V., Chudakov, Y. A., Ivanov, E. V. Formation of metal clusters in halloysite clay nanotubes. *Science and technology of advanced materials*. 2017; 18(1); 147-151.
13. Wilson, I., Keeling, J., Global occurrence, geology and characteristics of tubular halloysite deposits. *Clay Minerals*. 2016; 51(3); 309-324.
14. Nussbaum, S. R., Carter, M. J., Fife, C. E., DaVanzo, J., Haight, R., Nussgart, M., et al. An Economic Evaluation of the Impact, Cost, and Medicare Policy Implications of Chronic Nonhealing Wounds. *Value Health*. 2018; 21(1); 27-32.
15. Gupta, N., Gupta, S., Shukla, V., Singh, S. P. An Indian community-based epidemiological study of wounds. *Journal of wound care*. 2004; 13(8); 323-325.
16. Mahata, D., Jana, M., Jana, A., Mukherjee, A., Mandal, M. S., Saha, T., et al., Lignin-graft-Polyoxazoline Conjugated Triazole a Novel Anti-Infective Ointment to Control Persistent Inflammation. *Scientific Reports*. 2017; 7; 464.
17. Cheng, H., Frost, R. L., Yang, J., Liu, Q., He, J., Infrared and infrared emission spectroscopic study of typical Chinese kaolinite and halloysite. *Spectrochim Acta A: Molecular and Biomolecular Spectroscopy*. 2010; 77(5); 1014-1020.
18. Hahn, A. Fourier transform infrared spectroscopy model development, inferring biogeochemical properties for long sediment records from Southern Patagonia and Northeastern Siberia. *Journal of Paleolimnology*. 2019; 43(2); 247-259.
19. Samanta, S., Das, T., Ghorai, S., Chakraborty, S. K. Biocycling of Fractional Fatty Acid Components of Lipids in Mangrove-Benthic Systems, in Midnapore (East) Coast, India. 2018; 1(2).
20. Chakraborty, S. K. Interactions of environmental variables determining the biodiversity of coastal-mangrove ecosystem of West Bengal, India. *Water, Air, & Soil Pollution: Focus*. 2013; 251-265.
21. Chakraborty, S. K., Giri, S., Chakravarty, G., Bhattacharya, N. Impact of Eco-restoration on the Biodiversity of Sundarbans Mangrove Ecosystem, India. *Water, Air, & Soil Pollution: Focus*. 2009; 9(3); 303-320.
22. Chakraborty, S. K. Mangrove ecosystem of Sundarbans, India: Biodiversity, ecology, threats and conservation Mangroves: ecology, biology and taxonomy. NOVA Publishers, New York. 2011; 83-112.
23. Adrizzina, I., Adenin, L. I., Lubis, Y. M. Efficacy of Boric Acid as a Treatment of Choice for Chronic Suppurative Otitis Media and Its Ototoxicity. *Korean journal of family medicine*. 2018; 39(1); 2-9.
24. Gurtner, G. C., Werner, S., Barrandon, Y., Longaker, M. T. Wound repair and regeneration. *Nature*. 2008; 453; 314-321.
25. Yeh, C-J., Chen, C-C., Leu, Y-L. The effects of artocarpin on wound healing: in vitro and in vivo studies. *Scientific Reports*. 2017; 7(1); 15599.